

High-Fidelity Aeroelastic Optimization Benchmark Working Group: Benchmark Model and Problems

Alasdair C. Gray and Joaquim R. R. A. Martins
University of Michigan, Ann Arbor, MI, 48109

This document describes the benchmark model and optimization problems to be used by working group 1 for the special session on High-Fidelity Aeroelastic Design Optimization Applications and Benchmarks at the 2025 AIAA SciTech Forum. These were first proposed in our paper at the 2024 AIAA SciTech Forum [1]. This document contains the model and problem description sections of that paper, with some small changes. It should be considered the up to date reference for those planning to take part in the special session.

Contents

1 Wing Model	2
1.1 Wing Geometry	2
1.2 Aerodynamic Model	3
1.3 Structural Model	3
2 Optimization Problems	6
2.1 Objectives	6
2.2 Design Variables	8
2.2.1 Structural Variables	8
2.2.2 Geometric Variables	8
2.2.3 Aerodynamic Variables	9
2.3 Constraints	9
2.3.1 Structural Constraints	9
2.3.2 Geometric Constraints	10
2.3.3 Aerodynamic Constraints	11
3 Required Results	11
3.1 Benchmark Analyses	11
3.1.1 Benchmark Aerodynamic Analysis	11
3.1.2 Benchmark Structural Analysis	12
3.1.3 Benchmark Aeroelastic Analysis	12
3.2 Optimization Results	12
3.2.1 Case 1	12
3.2.2 Case 2	13
3.2.3 Case 3	13
A Appendices	14
A.1 XDSM Diagrams	14

1 Wing Model

1.1 Wing Geometry

The wing geometry is shown in figure 1. It consists of a single trapezoidal wing whose planform is based on the Boeing 717, with a uniform, untwisted RAE2822 cross-section¹, shown in figure 1c. This constant cross section extends up to the nominal semispan of 14 m, beyond which a small rounded tip cap extends a further 42.5 mm.

The wing contains a conformal wingbox with upper and lower skins, leading and trailing edge spars, and 23 ribs. The wingbox features a typical side of body (SOB) break at a semispan of $y = 1.5$ m, inboard of which the wingbox is unswept, resembling a center-box. Outboard of the SOB, the wingbox extends from 15 to 65 % of the chord. Four of the ribs are evenly spaced between the centerline and the SOB, the remaining ribs are evenly spaced between the SOB and the tip. The wingbox is subject to symmetry conditions at the centerline and is fixed in the chordwise and vertical directions at the SOB as shown in figure 1b.

CAD files of both the wing OML and wingbox geometries are provided in the repository.

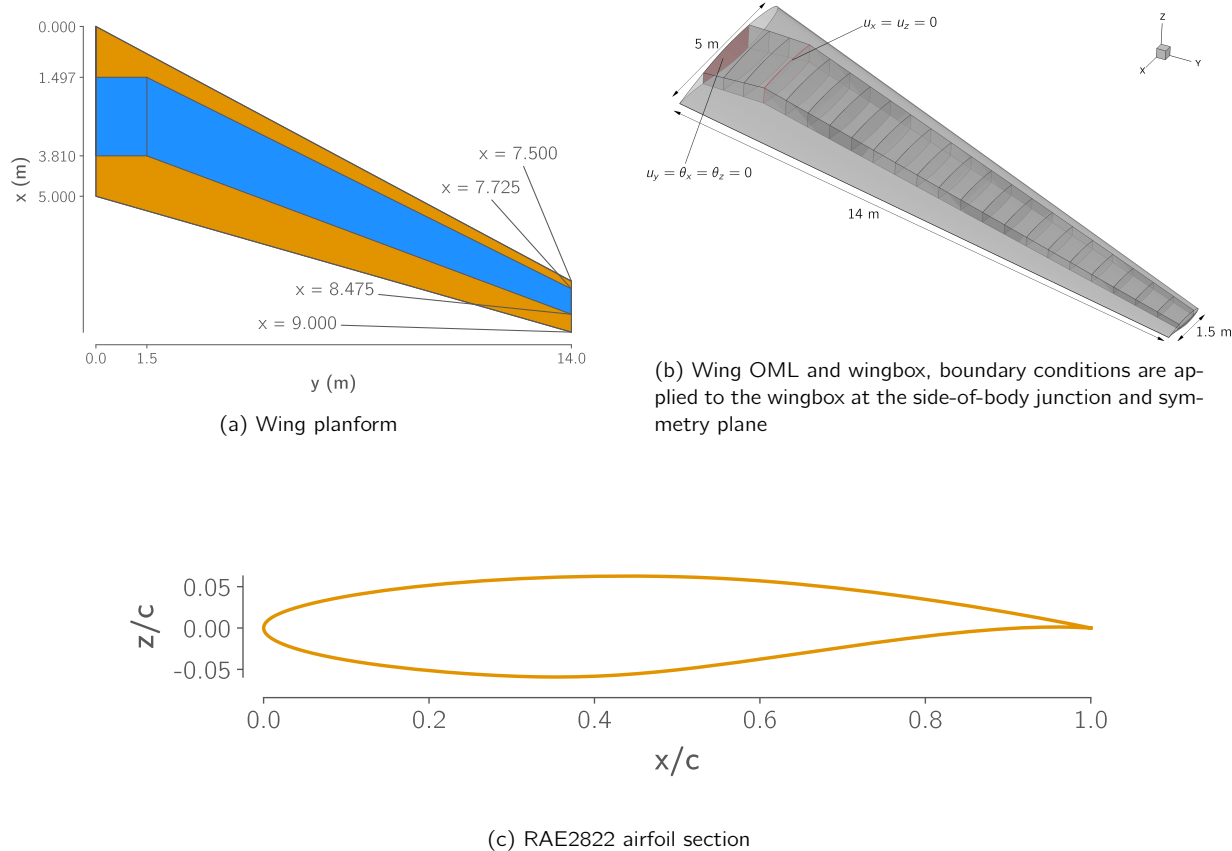


Figure 1: MACH tutorial wing OML and wingbox geometries.

¹This is the cross section for cuts through the wing on planes normal to the global Y-axis, rather than normal the quarter-chord axis.

1.2 Aerodynamic Model

A family of 3 structured multiblock computational fluid dynamics (CFD) meshes for the wing are provided in the repository, which are summarized in table 1. The finest mesh (L1) is intended only for mesh convergence and analysis studies, the L2 mesh is intended for final optimizations, and the L3 mesh for debugging. The coarser meshes are created by repeatedly coarsening the L0 surface mesh by a factor of 2 in each direction before extruding up to a distance of 300 m from the wing surface. The advantage of this approach is that it results in higher quality volume meshes than simply coarsening the L1 volume mesh. The disadvantage is that it does not provide the parametrically-similar series of grids necessary for a mathematically rigorous convergence study [2].

Use of these meshes is not required. Participants are encouraged to submit results using meshes with topologies and sizes that are suitable for their CFD codes and available computational resources.

Table 1: CFD mesh statistics.

Mesh	Cells	First cell height (m)	Target cruise y^+
L1	7.8×10^6	3×10^{-6}	0.125 – 0.25
L2	9.7×10^5	6×10^{-6}	0.25 – 0.5
L3	1.8×10^5	1.2×10^{-5}	0.5 – 1

1.3 Structural Model

A series of shell finite element (FE) meshes of the wingbox are also provided in the repository in BDF format. These are summarized in table 2 and consist of 4-node quad elements. Equivalent meshes with 9 and 16-node elements are also available in the repository however, these element types are not widely supported by commercial FE codes.

Table 2: FE mesh statistics.

Mesh	Elements between ribs	Elements between spars	Elements between skins	Total Elements	Total DOF ^a
L1	20	40	20	71,200	419,778
L2	10	20	10	17,800	103,158
L3	5	10	5	4,450	24,948
L4	3	5	3	1,401	7,536

^a Assuming six DOF per node.

To test the modeling capabilities relevant for analysis of modern aircraft structures, the wingbox is assumed to be made of stiffened composite panels. The stiffeners are assumed to have a T-shaped cross section, as shown in figure 4. The composite ply properties used throughout the wingbox are shown in table 3, taken from Brooks et al. [3]. Both the shell and stiffeners in every panel of the wingbox are assumed to consist of a $[0, -45, +45, 90]^\circ$ layup. Different layups of these plies are used for different components in the wingbox based on values used by Dillinger [4]. In the upper and lower skin shells and in all stiffeners, we assume a 0° biased layup with ply fractions of [44.41%, 22.2%, 22.2%, 11.19%], while in the spar and rib shells we use a more isotropic [10%, 35%, 35%, 20%]. In the skins, the stiffeners and 0° plies are aligned with the trailing edge spar, in the spars and ribs they are vertically oriented.

There are a wide variety of approaches to modeling stiffened shells in FE models and predicting their failure, particularly in the context of optimization. We therefore do not believe it is practical to enforce a single approach. However, the models used by participants should:

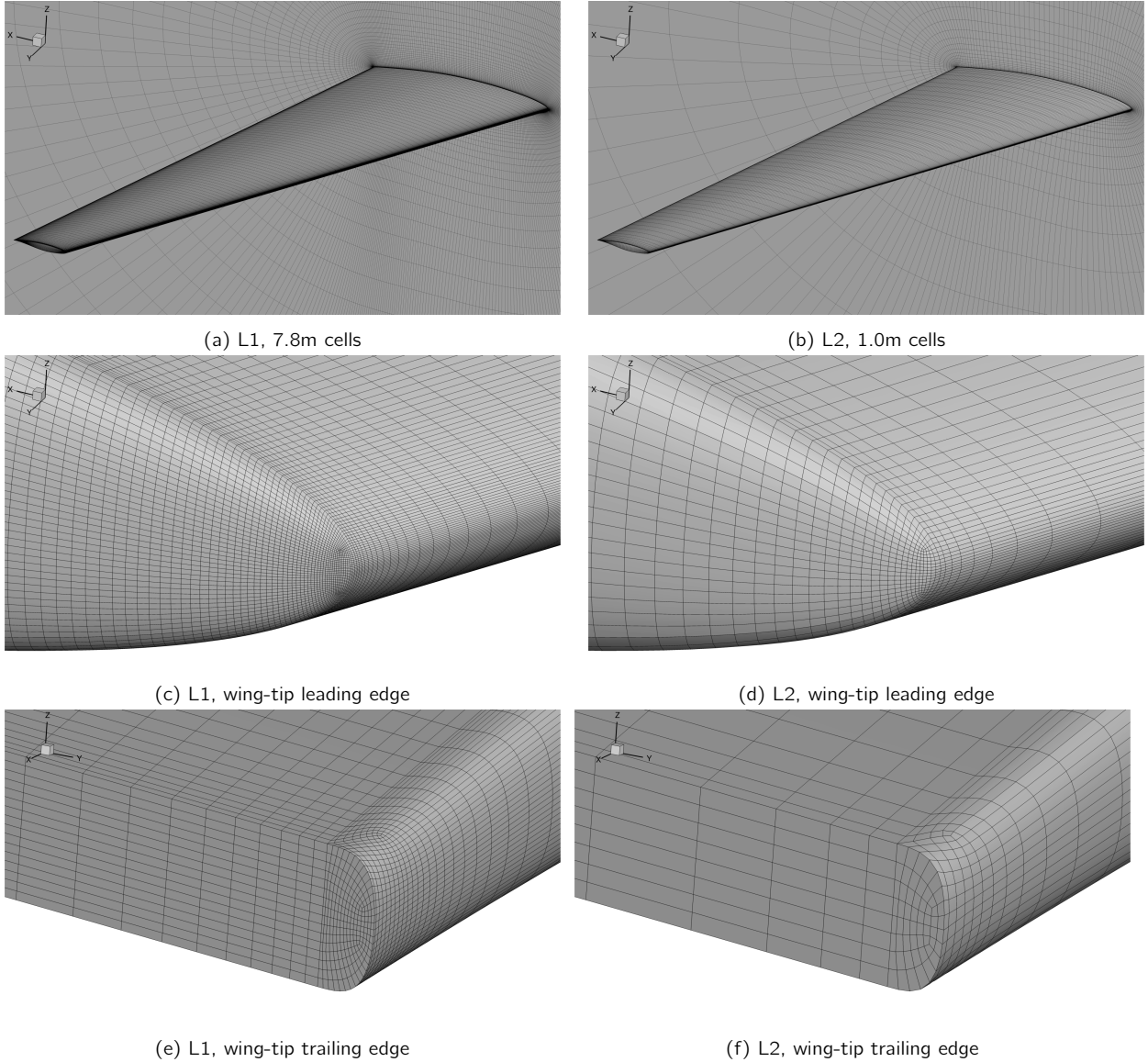


Figure 2: Structured multiblock CFD meshes provided for the benchmark model.

1. Be able to model the anisotropic composite laminate properties given above.
2. Be able to model the presence of panel stiffeners and, ideally, be able to parameterize their cross-section.
3. Use sufficient failure criteria to constrain that the structure has a safety factor of at least 1.5 to both material and buckling failure.

In all flight conditions, the structural model is subject to aerodynamic forces and the wingbox's self-weight. For the sake of simplicity, we do not include any inertial forces due to non-structural masses such as fuel, or leading and trailing edge devices. Although such loads are simple enough to include in a standalone analysis, they are difficult to include in an optimization problem due to the need to keep them consistent with the wing's geometry as it changes.

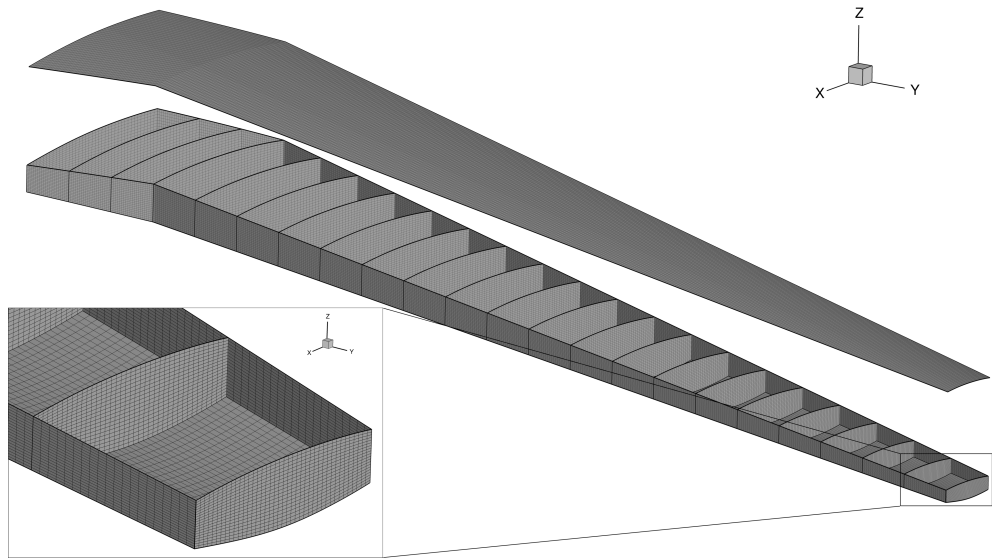


Figure 3: The finest wingbox mesh contains 71,200 quadrilateral elements and 419,778 DOF.

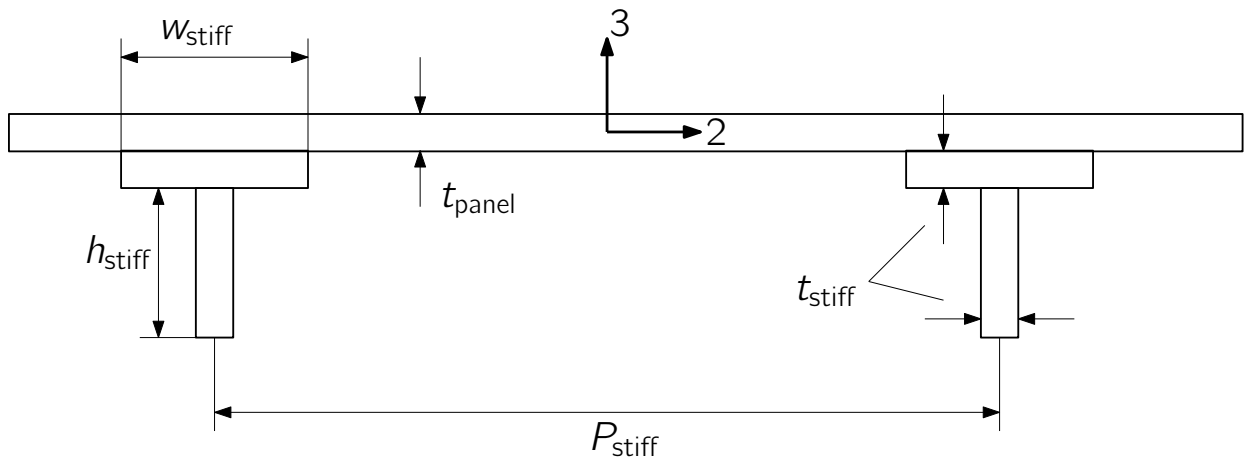


Figure 4: Stiffener cross-section.

Table 3: Composite ply properties

Property	Description	Value
E_{11}	Fiber direction modulus	117.7 GPa
E_{22}	Transverse modulus	9.7 GPa
G_{12}	In-plane shear modulus	4.8 GPa
G_{13}	Transverse shear modulus	4.8 GPa
G_{23}	Transverse shear modulus	4.8 GPa
T_1	Fiber direction tensile strength	1648 MPa
C_1	Fiber direction compressive strength	1034 MPa
T_2	Transverse tensile strength	64 MPa
C_2	Transverse compressive strength	228 MPa
S_{12}	Shear strength	71 MPa
ν_{12}	Major Poisson's ratio	0.35
ρ	Density	1550 kg m ⁻³

2 Optimization Problems

This section describes our three proposed benchmark optimization problems to be applied to the model just described. The three problems build on one another with the intention of allowing researchers to test their tools on increasingly complex problems:

Case 1: Structural mass minimization with a fixed geometry.

Case 2: Fuel burn minimization with a fixed wing planform.

Case 3: Fuel burn minimization with a variable wing planform.

Tables 4 and 5 list information about the aircraft and the flight conditions used in the optimization problems, which are all based on publicly available data on the high gross-weight variant of the Boeing 717.

2.1 Objectives

The objective function to be minimized in Case 1 is the wingbox mass, computed from the FE model. The objective function for cases 2 and 3 is the fuel burn over a given mission. The fuel burn is computed using a two-stage process that accounts for the fuel burn in both cruise and climb. This process starts by computing the landing gross mass (LGM):

$$LGM = M_{payload} + M_{frame} + M_{fuel, res} + 2M_{wing} \quad (1)$$

The total mass of a single wing is computed using the regression model created by Elham [5]:

$$M_{wing} = 10.147 M_{wingbox}^{0.8162} \quad (2)$$

Where $M_{wingbox}$ is the wingbox mass. Assuming the fuel burn during descent and landing is negligible, the mass at the start of the cruise phase, and then the takeoff gross mass (TOGM) are computed by

Table 4: Aircraft and mission specifications, based on the Boeing 717 high gross-weight variant.

	Quantity	Description	Value
Baseline wing geometry			
	b	Semispan	14 m
	C_{root}	Root chord	5 m
	C_{tip}	Tip chord	1.5 m
	S	Planform area (single wing)	45.5 m ²
	MAC	Mean aerodynamic chord	3.25 m
Masses			
	M_{payload}	Payload mass	14.5×10^3 kg
	M_{frame}	Operating empty mass (minus wing)	25×10^3 kg ^a
	$M_{\text{fuel, res}}$	Reserve fuel mass	2×10^3 kg
Fuelburn calculation parameters			
	R	Nominal range	3815 km
	R_{climb}	Climb segment range	290 km
	V_{climb}	Average climb speed	350 mph
	$C_{D,\text{frame}}$	Airframe drag coefficient (fuselage + tail + nacelle)	0.0152 ^b
	k_{tank}	Assumed fraction of wingbox that can store fuel	0.85
	V_{aux}	Auxilliary fuel tank volume	2.763 m ³
	TSFC	Thrust specific fuel consumption	18×10^{-6} kg N ⁻¹ s ^c
	ρ_{fuel}	Fuel density	804 kg m ⁻³

^a Approximated based on true empty weight of 31.1×10^3 kg.

^b Computed using a conceptual design drag build-up

^c Publicly available value for the Rolls-Royce BR700, a close relative of the 717's BR715 engine

Table 5: Flight conditions

Flight point	Altitude	Mach Number	Load factor	Aircraft mass
Cruise	10 400 m	0.77	1	$\sqrt{M_{\text{cruise, start}} \times LGM}$
Pull-up Maneuver	0 m	0.458	2.5	LGM
Push-down Maneuver	0 m	0.458	-1	LGM

rearranging the Breguet range equation:

$$M_{\text{cruise, start}} = LGM \exp \left(\frac{R \times TSFC}{V_{\text{cruise}}} \left(\frac{D_{\text{cruise}}}{L_{\text{cruise}}} \right) \right) \quad (3)$$

$$\text{TOGM} = M_{\text{cruise, start}} \exp \left(\frac{R_{\text{climb}} \times TSFC}{V_{\text{climb}}} \left(\frac{\cos(\gamma)}{L_{\text{cruise}}/D_{\text{cruise}}} + \sin(\gamma) \right) \right) \quad (4)$$

$$FB = \text{TOGM} - LGM \quad (5)$$

Where γ is the climb angle, here computed based on the assumed climb range and cruise altitude given in tables 4 and 5. The lift and drag in the cruise condition are computed using an aeroelastic analysis, the values are doubled to get the full aircraft values, and the drag of un-modeled components (fuselage, tail, and nacelles) is added:

$$L_{\text{cruise}} = 2L_{\text{wing}} \quad D_{\text{cruise}} = 2 \left(D_{\text{wing}} + \frac{1}{2} q_{\text{cruise}} S C_{D,\text{frame}} \right) \quad (6)$$

Where $C_{D,\text{frame}}$ is estimated using a conceptual drag build-up implemented by Adler and Martins [6] based on the methods of Torenbeek [7] and Raymer [8]. The area used in the above equation is the planform area of the baseline geometry and does not vary during optimization since we assume that the remainder of the aircraft remains identical.

2.2 Design Variables

The primary differences between the three benchmark problems are the amount of design freedom given to the optimizer through the design variables. Table 6 summarizes these design variables. Note that, the exact number and form of some design variables will depend on the structural modeling and geometric parameterization approaches used, as is explained in the following sections.

Table 6: Design variables to be used in the benchmark problems

Variable	Case 1	Case 2	Case 3
Structural sizing	✓	✓	✓
Pull-up maneuver angle of attack	✓	✓	✓
Push-down maneuver angle of attack	✓	✓	✓
Cruise angle of attack		✓	✓
Twist distribution		✓	✓
Section shapes		✓	✓
Chord distribution			✓
Span			✓
Sweep			✓

2.2.1 Structural Variables

Due to the variety of structural modeling approaches we want to support in these benchmark problems, we do not prescribe a specific set of structural sizing variables. Instead we specify the following requirements for the parameterization of the wingbox:

- A stiffener pitch of 150 mm should be used on all panels.
- Each rib, and each skin and spar segment between a pair of ribs, should be treated as a separate panel with its own structural sizing variables, as shown in figure 5.
- The parameterization should allow the optimizer to vary the thickness of the panels.
- The parameterization should allow the optimizer to at least vary the thickness of stiffeners (e.g if the stiffeners are modelled explicitly with shell elements), and ideally also their cross-section geometry².

This structural parameterization should remain the same for all three optimization problems.

2.2.2 Geometric Variables

In Case 1, the wing geometry is fixed and thus there are no geometric design variables. In Case 2, the section shapes of the wing may be changed in the z direction, and the twist distribution may be varied. In Case 3, the optimizer may also vary the span, sweep, and chord distribution. The parameterization method used to achieve these changes (e.g free-form deformation (FFD), CAD etc) and the level of detail (e.g number of values used to define the twist distribution) are left free. However, the following requirements must be satisfied:

- The twisting must occur about the leading edge of the wing.

²If parameterizing the stiffener cross-section, we recommend participants link the flange width, W_{stiff} , to the web height, h_{stiff} (e.g keeping $w_{\text{stiff}} = h_{\text{stiff}}$) rather than treating it as a separate variable.

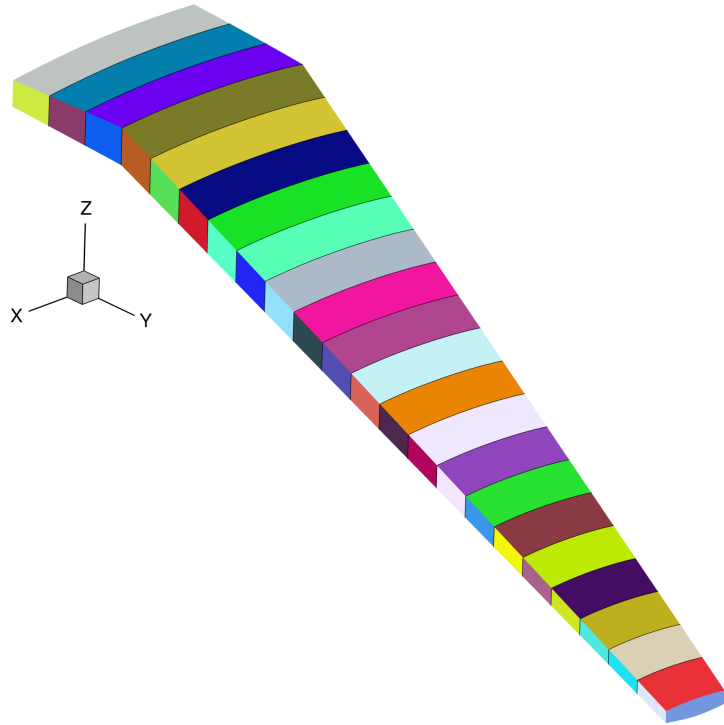


Figure 5: Each separately colored wingbox panel should be given its own structural sizing variables.

- The root of the wing (at the symmetry plane) must not be twisted.
- The shape changes must be parameterized in a manner that does not allow the optimizer to achieve twisting of the section shapes.
- The SOB junction of the wingbox should not move in the y direction.
- The leading edge of the wing must remain straight, save for a potential break at the SOB junction.

2.2.3 Aerodynamic Variables

Finally, the optimizer can control the angles of attack at each flight point to meet the lift constraints described in section 2.3.

2.3 Constraints

Table 7 provides a high-level summary the constraints applied in the 3 benchmark problems. As with the design variables, the exact formulation of the constraints in each benchmark problem will depend to some extent on the structural modeling and geometric parameterization approaches used by participants.

2.3.1 Structural Constraints

The primary structural constraints enforce that the wingbox has a safety factor of 1.5 to both material and buckling failure in both maneuver flight conditions. How this is achieved is left free.

Adjacency constraints are enforced to avoid abrupt changes in panel sizing. The change in panel and stiffener thicknesses between adjacent skin and spar panels³ is limited to 2.5 mm and the change in stiffener height to 10 mm. Some basic structural sizing rules suggested by Kassapoglou [9] should be used on all panels:

- The skin and stiffener thicknesses should be at least 0.6mm
- The stiffener heights should be at least 18mm
- The stiffener flange widths should be at least 25.4mm
- The aspect-ratio of the stiffener web ($h_{\text{stiff}}/t_{\text{stiff}}$) should be between 5 and 30.
- The thickness of the stiffener flanges on a panel should be no more than 15 time the panel thickness.
- The stiffener flange width should be less than the stiffener pitch to avoid overlapping.

Participants should enforce as many of these constraints as are applicable to their structural sizing parameterization in all three benchmark problems.

2.3.2 Geometric Constraints

Since the benchmark problems consider a limited selection of flight points, additional geometric constraints are required to ensure the optimizer produces a realistic wing geometry:

- The wing's leading edge radius must be at least 90% of its baseline value throughout the span to maintain reasonable low-speed performance.
- The front and rear spars must be at least 75% of their baseline height throughout the span to maintain the space required to mount components such as control surface actuators [10].
- The region between the rear spar and the trailing edge must be at least 50% of its baseline thickness to prevent the optimizer creating an unrealistically thin trailing edge.
- The wingbox volume must be large enough to store the amount of fuel required for the mission, as computed in the objective function.
- When the planform is varied, the wing loading (TOGM/2S) must be no greater than 600 kg m^{-2} .

When computing the fuel volume constraint, the total available fuel tank volume is the auxiliary tank volume plus the fraction of both wingboxes that is assumed to be available for fuel storage, the constraint can therefore be written as:

$$M_{\text{fuel}}/\rho_{\text{fuel}} \leq V_{\text{aux}} + 2k_{\text{tank}}V_{\text{wingbox}}$$

or:

$$\frac{M_{\text{fuel}}/\rho_{\text{fuel}} - V_{\text{aux}}}{2k_{\text{tank}}V_{\text{wingbox}}} \leq 1$$

which is better scaled. Note that the total fuel mass, M_{fuel} , is the sum of the fuel burn computed using equation 5 and the reserve fuel mass given in table 4.

³By this we mean that the difference between variables on two adjacent skin panels, or two adjacent spar panels, are constrained, but not the difference between a spar panel and an adjacent skin panel.

2.3.3 Aerodynamic Constraints

The lift produced by the wing at each flight point must be equal to the aircraft weight multiplied by the relevant load factor. The maneuvers are assumed to be performed at the TOGM since the inertial relief of the fuel is not included in our structural model. The aircraft mass for the cruise condition is taken to be the mid-cruise mass, which is the geometric average of the cruise start and end masses. This accounts for the non-uniform rate of fuel burn over the segment.

Table 7: Constraints to be enforced in the benchmark problems

Function	Description	Included in		
		Case 1	Case 2	Case 3
$SR_{2.5g} \leq 1/1.5$	Pull-up maneuver strength ratio	✓	✓	✓
$SR_{-1g} \leq 1/1.5$	Push-down maneuver strength ratio	✓	✓	✓
$ t_{\text{panel},i} - t_{\text{panel},j} \leq 2.5 \text{ mm}$	Skin/spar panel thickness adjacency	✓	✓	✓
$ t_{\text{stiff},i} - t_{\text{stiff},j} \leq 2.5 \text{ mm}$	Skin/spar stiffener thickness adjacency	✓	✓	✓
$ h_{\text{stiff},i} - h_{\text{stiff},j} \leq 10 \text{ mm}$	Skin/spar stiffener height adjacency *	✓	✓	✓
$t_{\text{stiff},i} \leq 15t_{\text{panel},i}$	Maximum stiffener thickness *	✓	✓	✓
$h_{\text{stiff},i} \leq 30t_{\text{stiff},i}$	Maximum stiffener aspect-ratio *	✓	✓	✓
$h_{\text{stiff},i} \geq 5t_{\text{stiff},i}$	Minimum stiffener aspect-ratio *	✓	✓	✓
$w_{\text{stiff},i} \leq p_{\text{stiff},i}$	Minimum stiffener spacing *	✓	✓	✓
$L_{2.5g} = 2.5LGMg$	Pull-up maneuver lift level	✓	✓	✓
$L_{-1g} = -LGMg$	Push-down maneuver lift level	✓	✓	✓
$L_{\text{cruise}} = M_{\text{mid-cruise}}g$	Cruise maneuver lift level	✓	✓	✓
$t_{\text{spar}} \geq 0.75t_{\text{spar},0}$	Minimum Spar height	✓	✓	✓
$t \geq 0.5t_0$	Minimum TE thickness	✓	✓	✓
$R_{\text{LE}} \geq 0.9R_{\text{LE},0}$	Minimum Leading edge radius	✓	✓	✓
$M_{\text{fuel}}/\rho_{\text{fuel}} \leq V_{\text{aux}} + 2k_{\text{tank}}V_{\text{wingbox}}$	Fuel volume	✓	✓	✓
$TOGM/2S \leq 600 \text{ kg m}^{-2}$	Maximum wing loading	✓		

* May not be applicable depending on structural parameterization.

3 Required Results

3.1 Benchmark Analyses

In order to quantify the differences between the codes and meshes used by participants separately from differences in optimized designs, participants should provide the following results for the baseline wing. These analyses should be performed using the same meshes participants use for their optimizations. They should be performed using the baseline geometry and the following structural sizing variables on every panel:

3.1.1 Benchmark Aerodynamic Analysis

Report the values of C_L and C_D for the baseline OML in the cruise condition at angles of attack from 0 to 5° in steps of at most 1°.

Variable	Value (m)
Stiffener Pitch	0.15
Panel Thickness	0.0065
Stiffener Height	0.05
Stiffener Thickness	0.006

3.1.2 Benchmark Structural Analysis

Simulate the baseline wing under a uniform pressure load of 30 kPa applied to the lower skin of the wingbox, do not include inertial (a.k.a self-weight) loads. Report the tip deflection and twist, compliance (total strain energy), and separate factors of safety for material and buckling failure. The tip deflection and twist should be calculated using the deflections at the top corners of the tip rib, as shown in figure 6.

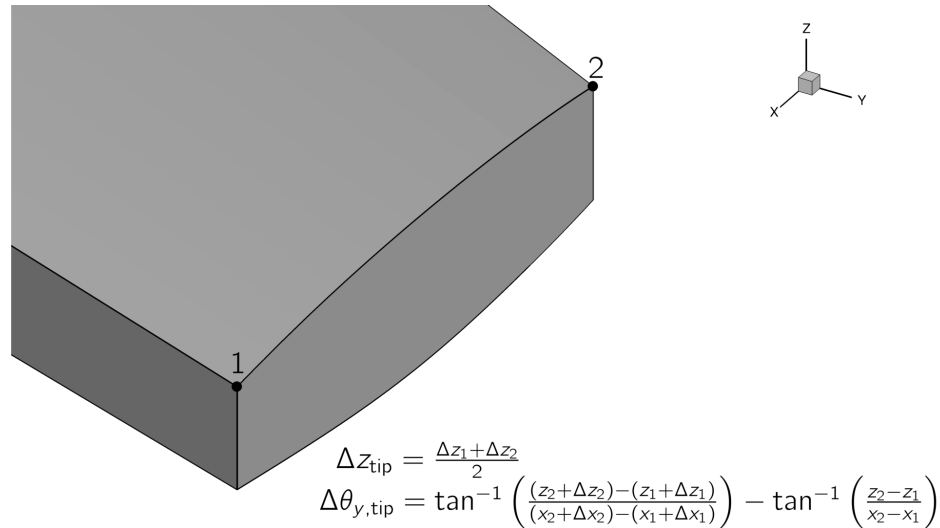


Figure 6: Method for calculating wing tip deflections.

3.1.3 Benchmark Aeroelastic Analysis

Perform aeroelastic analyses of the baseline wing at the two maneuver conditions used in case 1, include inertial (a.k.a self-weight) loads proportional to the load factor for each flight point. Use an angle of attack of -6.4° for the push-down maneuver and 10.3° for the pull-up maneuver. For each flight condition, report the single wing lift value, and the same values reported for the benchmark structural analysis.

3.2 Optimization Results

Participants solving the benchmark optimization problems should provide the following results at a minimum:

3.2.1 Case 1

- Wall clock time and total number of CPU hours required for each optimization and a brief description of the hardware used.

- Convergence plots showing the objective value along with measures of constraint violation and optimality vs iterations, function evaluations, or wall time. The criteria used to terminate the optimization should also be described.
- Spanwise lift distribution plots for the initial and optimized designs in all flight conditions.
- Plots of the spanwise structural sizing distributions in the upper and lower skins, and the leading and trailing edge spars. Participants should plot the equivalent axial thickness, which is the thickness of an unstiffened panel with the same axial stiffness as the stiffened panel⁴.
- Quantities of interest for the optimized design:
 - Wingbox structural mass
 - Wing total mass
 - Aircraft landing gross mass
 - Angle of attack in each maneuver condition

3.2.2 Case 2

As for Case 1 plus:

- Plots of in-flight twist distributions for each flight condition for the initial and optimized designs.
- Airfoil shapes and cruise Cp distributions of initial and optimized designs at 10, 30, 50, 70 and 90% semispan locations.
- Additional quantities of interest for the optimized design:
 - Cruise angle of attack
 - Cruise lift-to-drag ratio (including airframe drag)
 - Total fuel burn
 - Take-off gross mass
 - Fuel tank usage $\left(\frac{M_{fuel}/\rho_{fuel} - V_{aux}}{2k_{tank}V_{wingbox}} \right)$
 - Lift to drag ratio for the optimized wing for a range of $\pm 1^\circ$ angle of attack and ± 0.02 Mach number relative to the cruise condition. Participants should simulate at least the 9 points shown in figure 7, but may choose to simulate more points within the range if desired.

3.2.3 Case 3

As for Case 2 plus:

- Additional quantities of interest for the optimized design:
 - Wing semispan
 - Wing aspect ratio

⁴This can be computed as $t_{eq} = t_{panel} + A_{stiff}/P_{stiff}$, where t_{panel} is the panel thickness, A_{stiff} is the stiffener cross-sectional area, and P_{stiff} is the stiffener pitch.

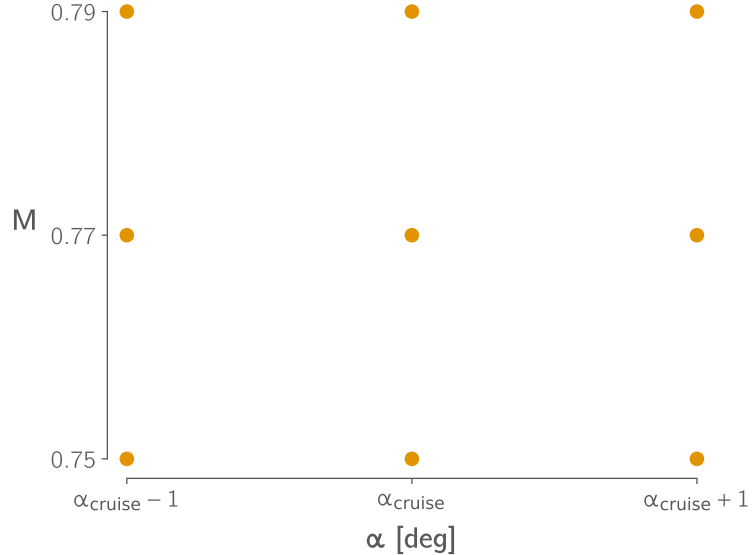


Figure 7: Minimum required stencil for the post-optimality study.

- Wing taper ratio
- Wing leading edge sweep angle
- Wing area
- Wing loading

A Appendices

A.1 XDSM Diagrams

Figures 8 to 10 show XDSM diagrams for the case 2 & 3 benchmark problems. Figure 8 shows the top-level XDSM for the optimization problems, figure 9 shows the XDSM inside each aerostructural analysis block, and figure 10 shows the XDSM for the aircraft performance block.

For case 1, the XDSMs are almost identical, with the cruise flight point removed, and the fuel burn and all dependent calculations removed from the aircraft performance component.

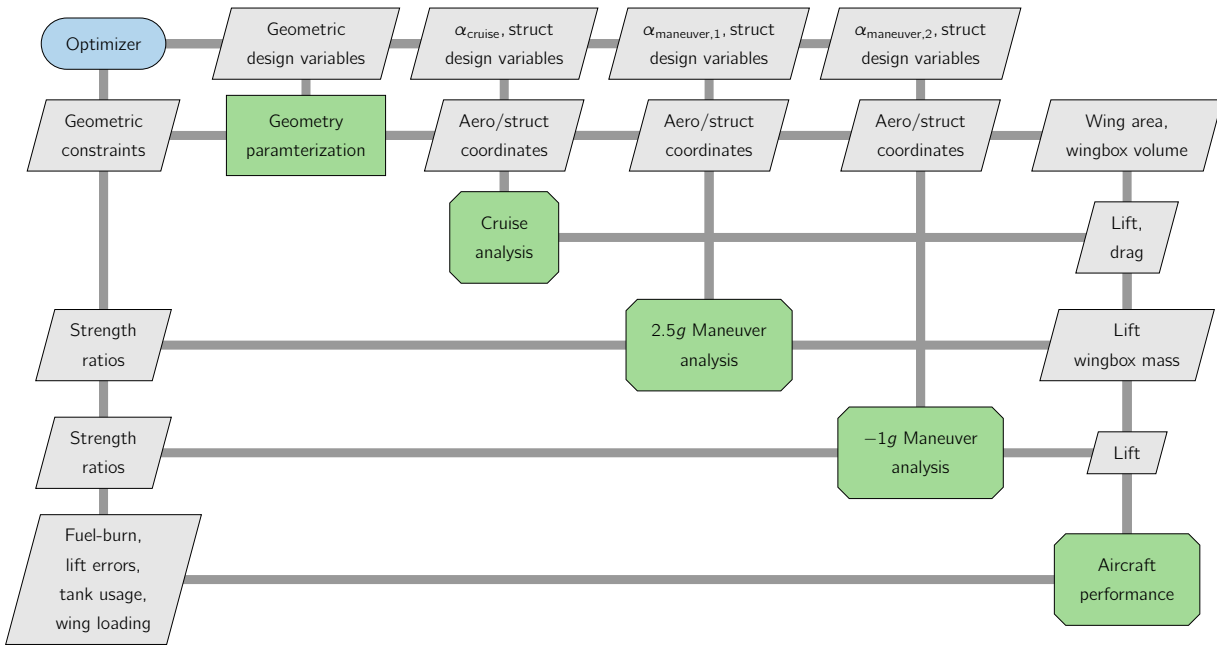


Figure 8: Top level XDSM for the case 2 & 3 benchmark problems.

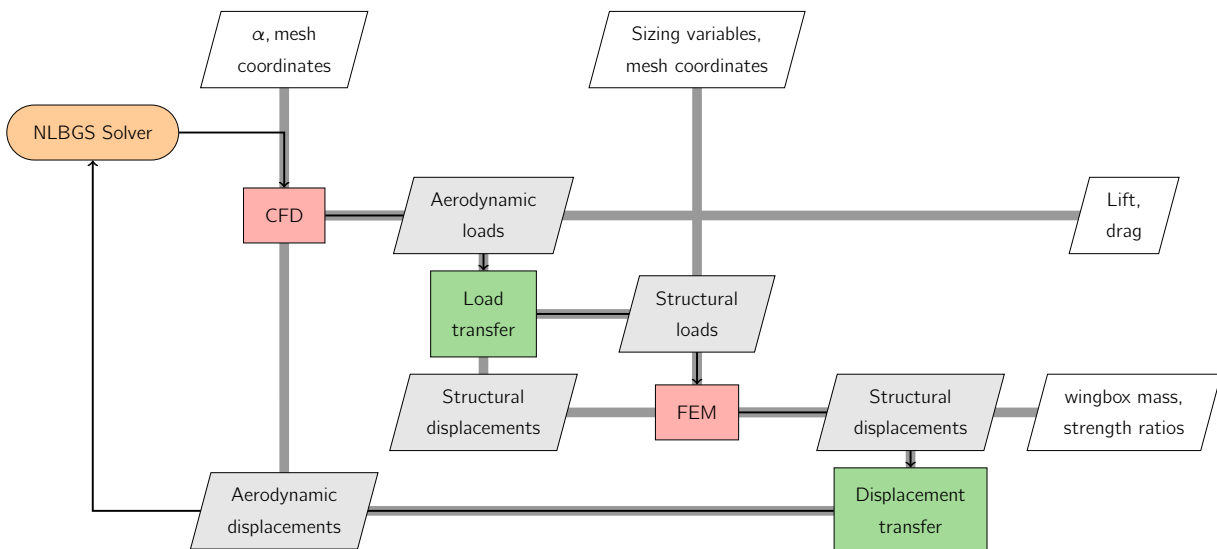


Figure 9: XDSM for the aerostructural analysis at each flight point.

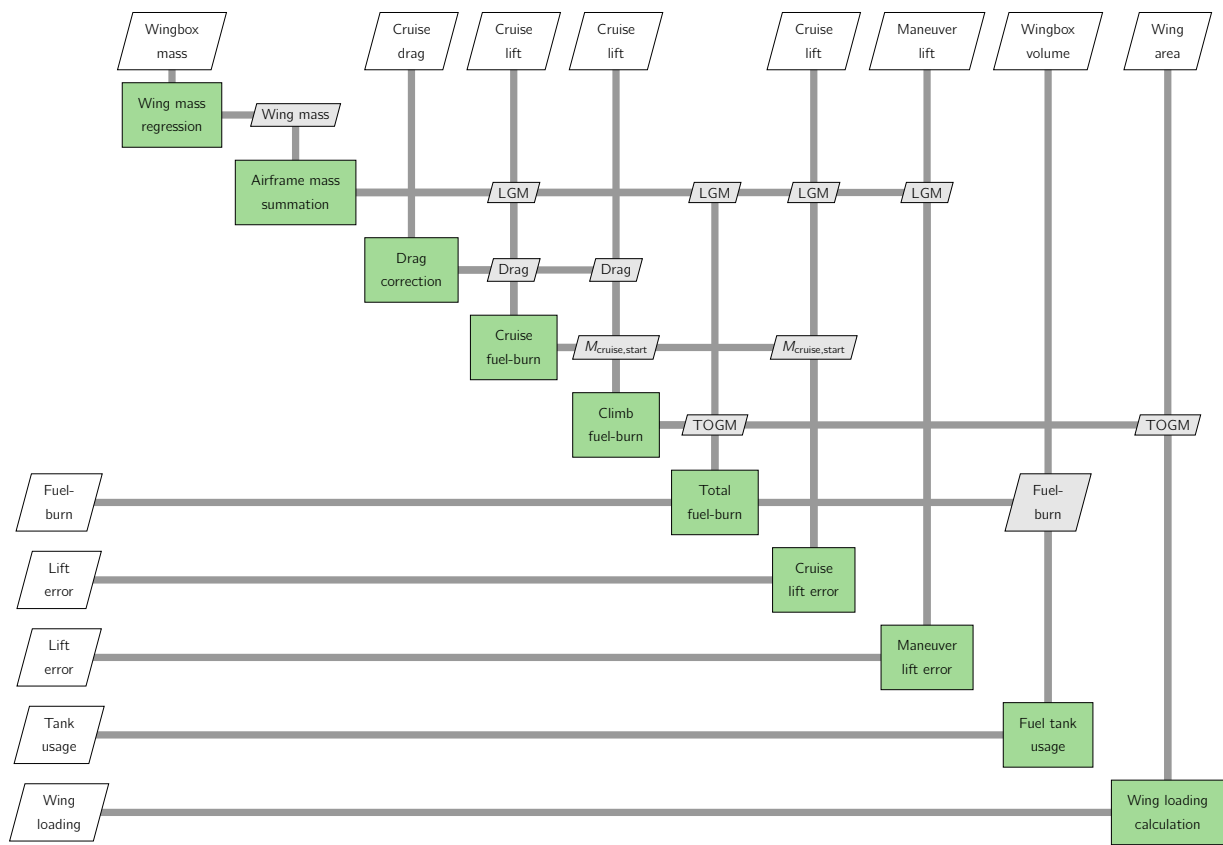


Figure 10: XDSM for the aircraft performance analysis component.

References

- [1] Gray, A. C., and Martins, J. R. R. A., "A Proposed Benchmark Model for Practical Aerostructural Optimization of Aircraft Wings," *AIAA SciTech Forum*, Orlando, FL, 2024. doi:10.2514/6.2024-2775.
- [2] Vassberg, J., "A Unified Baseline Grid about the Common Research Model Wing/Body for the Fifth AIAA CFD Drag Prediction Workshop (Invited)," *29th AIAA Applied Aerodynamics Conference*, 2011. doi:10.2514/6.2011-3508.
- [3] Brooks, T. R., Martins, J. R. R. A., and Kennedy, G. J., "Aerostructural Trade-offs for Tow-steered Composite Wings," *Journal of Aircraft*, Vol. 57, No. 5, 2020, pp. 787–799. doi:10.2514/1.C035699.
- [4] Dillinger, J. K. S., "Static Aeroelastic Optimization of Composite Wings with Variable Stiffness Laminates," Ph.D. thesis, TU Delft, 2014. doi:10.4233/uuid:20484651-fd5d-49f2-9c56-355bc680f2b7.
- [5] Mariens, J., Elham, A., and Van Tooren, M. J., "Influence of weight modelling on the outcome of wing design using multidisciplinary design optimisation techniques," *Aeronautical Journal*, Vol. 117, No. 1195, 2013, pp. 871–895. doi:10.1017/S0001924000008563.
- [6] Adler, E. J., and Martins, J. R. R. A., "Blended wing body configuration for hydrogen-powered aviation," *AIAA Aviation 2023 Forum*, 2023. doi:10.2514/6.2023-4020.
- [7] Torenbeek, E., *Synthesis of Subsonic Airplane Design*, 6th ed., Delft University Press and Kluwer Academic Publishers, 1990.
- [8] Raymer, D. P., *Aircraft Design: A Conceptual Approach*, 2nd ed., AIAA, 1992.
- [9] Kassapoglou, C., *Design and Analysis of Composite Structures: With Applications to Aerospace Structures*, 2nd ed., John Wiley & Sons Ltd, 2013. doi:10.1002/9781118536933.
- [10] Liem, R. P., Kenway, G. K. W., and Martins, J. R. R. A., "Multimission Aircraft Fuel Burn Minimization via Multipoint Aerostructural Optimization," *AIAA Journal*, Vol. 53, No. 1, 2015, pp. 104–122. doi:10.2514/1.J052940.